Acoustic interaction as a primary cause of infrasonic spinning mode generation and propagation from wind turbines. Kevin A. Dooley (Kevin Allan Dooley Inc. Toronto, Ontario, Canada) Andy Metelka (Sound and Vibrations Solutions Inc. Acton, Ontario, Canada)

Relatively balanced load related pressure waves from the rear surface of each rotor blade, are at a frequency of 1 per revolution of the turbine and are phase shifted by 120 degrees from each other. The superpositions of these infrasonic waves destructively interfere. This action results in a non-propagating rotor locked mode, however, the shielding (reflecting) effect of the tower as each blade passes, interrupts the balanced destructive interference for a small portion of rotor angle three times per revolution. The momentary un-balance between the destructive interfering waves, results in the generation of Tyler-Sofrin spinning mode series, which propagate into the far field. The spinning mode radiation angles, coupled with the low decay rate of infrasound, result in higher far field sound pressure levels than would be predicted for a point source. An analysis approach partially derived from Tyler-Sofrin (1962) is presented. Field microphone data including phase measurements identifying the spinning modes are also presented.

ACKNOWLEGEMENTS

The encouragement and many useful suggestions from Professor Colin Hanson and my colleague and friend Tatjana Pekovic in the preparation of this report were invaluable.
The many hours of stimulating and challenging discussion with my friend, business partner and colleague Mr. Elwood Morris will pay dividends for many years to come.

1. INTRODUCTION

This paper discusses Blade Passing Frequency (BPF) infrasound and its harmonics, although some results on Low Frequency Noise at discrete amplitude modulated frequencies at about 20 Hz plus harmonics is briefly discussed as being a side effect of the spinning mode generation mechanism. The initial analysis focuses on noise behind (downwind) the turbine, off axis radiation close to the turbine (at less than about 1 wavelength) is expected be affected by the differential distances between each of the rotating blades and the observation point, and require further analysis which is not covered in the study presented in this paper.
Other broadband noise generation mechanisms such as vortex or turbulence are not discussed. Atmospheric effects on the propagation of spinning modes and noise in general have not been included in this study but will clearly be required for a complete and accurate prediction of far field noise levels.

1.1 Background

Narrow band infrasonic Fast Fourier Transform (FFT) measurements inside homes situated close to some wind turbine installations show clear acoustic signatures at the BPF and harmonics, of the nearby wind turbines (Ref: 2.0, 4.0), (Figure 1). Multiple averaged Fast Fourier Transform (FFT) measurements show similar clearly identifiable acoustic signatures of wind turbine BPF harmonics at over 125 kilometers distance from the closest wind turbine installations (Fig 2 and Ref 4.0) at Sound Pressure Levels (SPL's) which have been measured to be within -25db of the SPL's recorded inside a home within 500 meters of a turbine installation (Fig 1 Fig 2 & Ref 4). These measurement results spurred an in-depth analysis of the infrasonic noise generation mechanisms involved at the turbine followed by close proximity (~200 meters) phase measurements at ground level near to a wind turbine (Figure 9 and Table 1).

2. GENERATING MECHANSIMS

Rotor alone Modes
As has been previously shown by J.M Tyler & T.G Sofrin in their mile-stone paper (Ref 1), a spinning rotor having a series of airfoil blades in air, produces a rapidly decaying spinning pressure pattern at the rotor, which they named a Spinning Mode.
The magnitude of the pressure peaks and rarefactions (lobes) are directly related to the differential pressure between the suction and pressure surfaces of the rotating blades (Ref 1-Fig.2). This rotating pressure pattern is referred to as a rotor alone mode (sometimes as a rotor locked mode) and decays as a function of axial distance (x) from the rotor.
The rotor alone mode spins with the same angular velocity as the rotor angular velocity ($\Omega = 2\pi N$), where (N) is rotor speed in revolutions per second. The rotor alone mode generates a fundamental frequency ($f = \mathrm{BN}$) plus harmonics, where B is the number of blades, and is represented by the Fourier series 1.1 (Ref 1.0).

$$p\,(\theta, t) = \sum_{n=1}^{\infty} a_n \cos[\, n(\theta - B\Omega t) + \emptyset_m \,] \qquad (1.1)$$

Where (a) and $(\emptyset)$ are amplitude and phase parameters required to synthesize the particular pressure wave, (n) is the harmonic number (positive integers) and B is the number of blades on the rotor.
The experimental work reported in Reference 1 confirmed the validity of equation 1 as providing an accurate formula for calculating the multi-lobed pressure pattern rotating at the rotor speed in a duct, when observed with a probe microphone close to the rotor face at a fixed radius and circumferential angle (θ), and as a function of time (t).

Rotor alone mode decay rate

The rotor alone mode SPL $[p\ (\theta, t)]$ was shown to decay exponentially (Ref 1) in a duct as a function of axial distance (x) from the rotor, when the tangential velocity of the rotor generated wave Center of Propagation (C.P.) is below the local speed of sound (c).
Such mode is referred to as being below cut-on or is cutoff, and for a particular compressor rotor in the Tyler Sofrin study (8 blades) was shown to decay at about -60db per radius of axial displacement (2.1). The very steep decay rate reduces abruptly; to an insignificant decay versus distance as the circumferential phase velocity or spin rate of the C.P. reaches the local velocity of sound, a condition referred to in Reference 1 as mode cut-on.

$$p(x) = p_0\ e^{-k_x x} \qquad \text{2.1(ref. 1.0)}$$

Where: $$k_x = 2\pi\sqrt{\left|\frac{1}{\lambda^2} - \frac{1}{\lambda_s^2}\right|} \qquad \lambda_s \leq \lambda \qquad \text{2.2 (ref. 1.0)}$$

And;
(x): = axial distance from the rotor plane
(λ): = the free field wavelength
(λ_s): = the circumferential wavelength at the rotor face, defined here as *[1]:

$$(\lambda_{s_m}) = 4Z_m \sin(\frac{\pi}{2\mathrm{m}}) \qquad \text{2.3}$$

Where: (Z_m) is the radial location of the center of the pressure pattern (m) on the rotor and (m) is the number of pressure cycles or the rotor harmonic number (Figure 3).

*[1] *In this study,* $(0.5\lambda_{s_m})$ *is in fact the straight-line distance between pressure centers (figure 3) as opposed to a curved line implied by the term "circumferential". The reference 1 definition of* $(\lambda_s = 2\pi r0/B)$*, where B is the blade count and (r0) is the duct radius, is insignificantly different from the definition chosen in this study for high blade counts, where with 8 blades the difference in results between the two definitions is less than 0.7%, however with a blade count of 3 the difference in the calculated distance between pressure centers is significant at over 4.5%. The error becomes progressively more significant at harmonic numbers less than 3.*

Figure 1 (below)

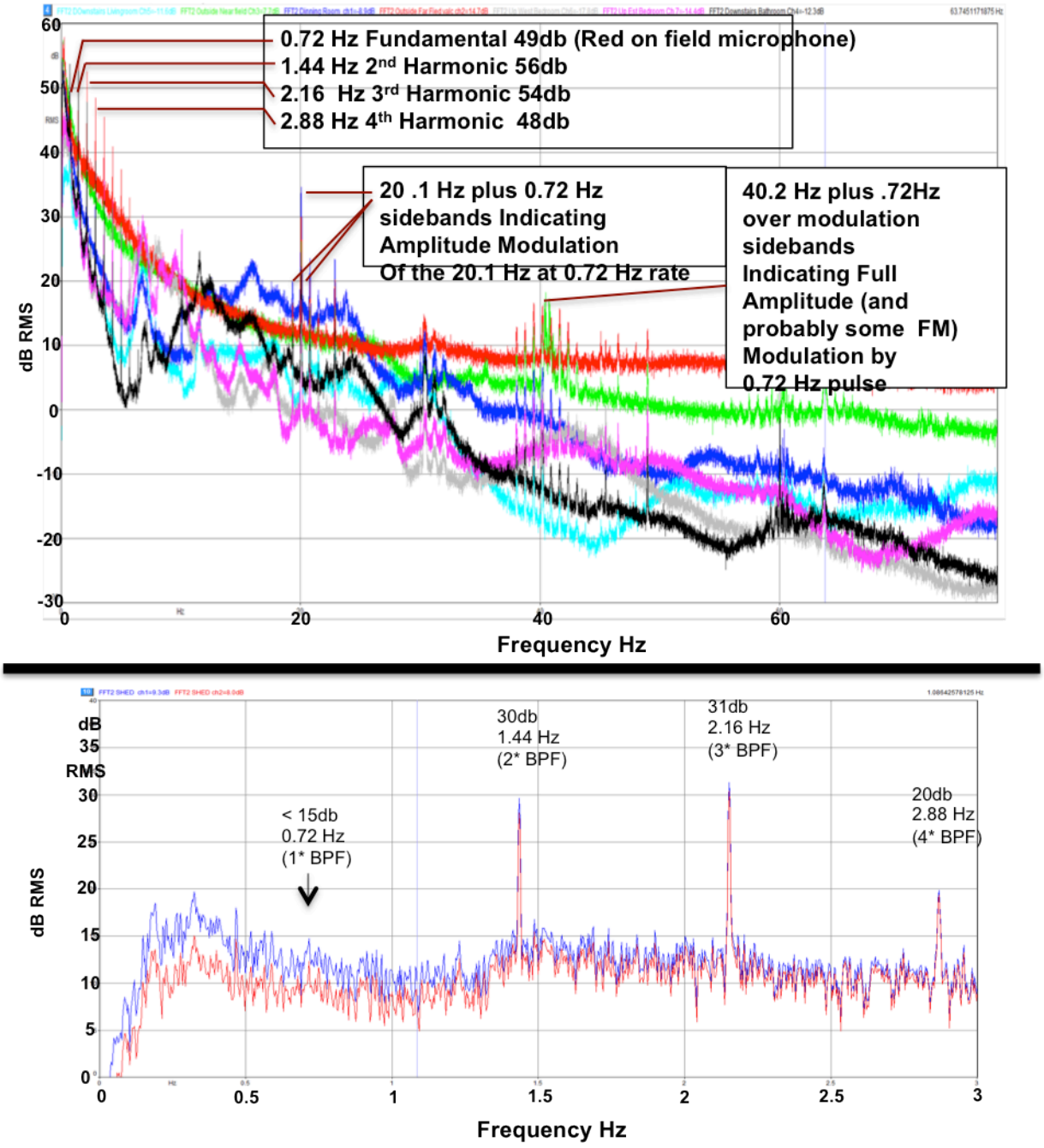

Figure 2

Figure 1 shows a frequency spectrum plot of 6 separate microphones recorded near Kincardine Ontario, July 2013 over a period of about 5 hours at night. The Red trace is data from an outside microphone located approximately 90 meters closer to the wind turbine than the house. The Green trace is from a microphone just outside the house. The remaining four microphones are located inside at various locations throughout the house (ref 4).

Figure 2 above is a spectrum plot of two microphones located together, recorded in Parry Sound Ontario, July 2013 over a duration of 1 hour at night, the location is more than **125 Km** *from the closest wind turbine (ref 4).*

2.2 Wind turbine rotor locked Fourier series

Equation 1.1 Fourier series (Ref 1) is an appropriate representation for a multi-bladed rotor where aerodynamic conditions around any given circumferential path are identical for all identically spaced blades, and was clearly sufficient for the compressor work being performed in Reference 1.
The wind turbines of interest are typically over 300 times the diameter of the compressor rotor studied in reference 1.0 and have less than one tenth the number of blades.
The relatively large radial span of wind turbine blades has the potential for the individual blades being exposed to independently varying aerodynamic conditions during a complete rotation, and as has been detailed in section 5.0 are certainly subject to independently varying acoustic conditions (Ref: 3). For the above reasons and in anticipation of further requirements to be discussed, the Fourier series representation has been re-defined for this study such that each of the 3 blades on the wind turbine rotor can be treated separately but also as a part of the same rotor system.
A revision of the pressure field expression $p\ (\theta, t)$ at the plane of the rotor at a fixed radius has been derived and is given by:

$$p\ (\theta,t) = \sum_{m=1}^{\infty} p_{m_i} \cos\left[m(\theta_i - \Omega t) + \phi_{m_i}\right]$$
$$+ \sum_{m=1}^{\infty} p_{m_{ii}} \cos\left[m(\theta_{ii} - \Omega t) + \phi_{m_{ii}}\right]$$
$$+ \sum_{m=1}^{\infty} p_{m_{iii}} \cos\left[m(\theta_{iii} - \Omega t) + \phi_{m_{iii}}\right] \qquad (3.1)$$

Each of the three terms of (3.1) separated by the Σ symbols represents a single turbine blade designated by the index i, ii, and iii (the Σ symbol is used here to indicate clearly where each blade term begins and becomes more useful in later sections as the expression is expanded). The blades are located at angles of nominally 2π/3 apart (120 degrees) defined by θ_B ($\theta_i, \theta_{ii}\ and\ \theta_{iii}$) and have effective differential surface pressure values $p_i\ p_{ii}\ and\ p_{iii}$.
Equation 3.1 describes the pressure pattern at the rotor plane at a fixed radius, as a function of time (t) and observer circumferential angle (θ), when the pressure amplitude coefficient (p) is given. The value of (p) is a function of the generator power output, blade design, wind speed, rotor speed, blade angle and radius of observation.
For downwind tower wind turbines the turbine blade passing frequency noise source studied in this paper is a rotor locked spinning mode source (3.1) generated as a result of the steady differential aerodynamic pressures (p) developed on the surfaces of the turbine blades as a function of wind speed, blade speed and blade angle (as opposed to an aerodynamic blade-wake/tower interaction noise generation mechanism which may also result in the generation of spinning modes).
The aerodynamically generated steady state blade surface pressures, acting in conjunction with an area of the blade averaged over a given radius from the turbine axis, generate the torque force input to the turbine generator system, and have been estimated based on the output power of a 1.6 MW rated

turbine generation system and a general understanding of the wind turbine speed and approximate dimensional specifications.

Based on the generally accepted active radius of the turbine blades being at about 80% of the blade span (Ref. 3) and assuming a +/-15% effective radial work span, the steady surface pressure differential on a hypothetical 40 meter radius 3 blade turbine is estimated be in the range of about 4500 Pa (Ref Appendix 1). The amplitude coefficient (p) for (m) = 60, was calculated (Ref Appendix 1) to be approximately -80 Pa (with no consideration for wind shear effects).

The circumferential pressure distribution implied by the Fourier series of 3.1 is illustrated in Figure 3.

Figure 3 (left hand side) is depicting a snapshot of the pressure pattern as it may be observed just rear of the rotor plane of a hypothetical 40 meter radius wind turbine, the discs representing the Low and High pressure regions (L & H) circumferentially distributed at the 80% radial location as they may be measured on a rotating, load balanced three blade wind turbine rotor.

The six discs of Figure 3 represent the area of the source pressure waves of the third harmonic (BPF) of rotor frequency of rotation (m=3), the points of contact between the discs represent the zero crossing point or atmospheric pressure and the center point of each disc represents the +pressure or – pressure peak.
The right hand image of Figure 3 is a representation of the same rotor pressure pattern snap shot recorded at a (spherical) plane rearward about 100mSec after the Figure 3 left hand snapshot (approximately 34 meters rearward from the rotor plane). The Figure 3 right-hand diagram depicts the normal dispersion of each of the pressure waves (with no tower interaction influence) as a function of time (x distance), resulting, hypothetically, in a partial destructive interference of each of the pressure waves with its neighboring waves (note that the destructive interference will affect the area of the pattern most towards the axis of rotation first).

3.0- Sound Pressure Level decay as a result of destructive interference (Hypothesis)

Although the study of Ref 1 measured and characterized the exponential SPL decay rate, an explicit physical mechanism for the decay was not given.
A hypothesis presented here, identifies a possible physical mechanism for the decay of the rotor alone mode for an open (un-ducted) rotor.
In this study of a large duct-less wind turbine rotor, the decay effect of the (open) rotor locked modes is attributed to the destructive interference between each of the identical rotor sourced pressure lobes with every other virtually identical pressure lobe, and occurs over the axial distance required for normal spherical dispersion of each lobe into the space occupied by adjacent lobes (Figure 3 and equation 3.3).
The relatively short circumferential distance between rotor blade generated pressure peaks and rarefactions (circumferential half wavelength $0.5\lambda_s$), relative to the free field half wavelength (0.5λ) of the same frequency pressure waves, evidently governs the destructive interference between the waves as a function of distance from the source (the rotor blades)*[2].

*[2] *The destructive interference phenomena is expected be an intrinsic effect associated with any symmetrical subsonic rotor, however, because it occurs over a relatively short axial distance on small high-speed propellers or fans, direct evidence of this phenomenon may generally not be easily measurable beyond about one diameter or so from the plane of an open rotor, where high velocity air-*

flow conditions may impede practical measurements, possibly obscuring the obvious detection of the effect.

3.2 Open Rotor decay rate based on the destructive interference hypothesis:

The decay by destructive interference hypothesis essentially states that the overlap between the circumferentially distributed pressure centers (Fig. 3 right hand image) of a given rotor locked mode (m) will, increase as a function of distance (c * t), resulting in a progressive destructive interference between the pressures centers as a function of distance. This is a result of the angle between the opposing pressure centers being fixed by the harmonic number (m), and the radius at which the mode is located on the rotor (Z_m), however, the angle between the opposing pressure boundaries is a function of the radius of the pressure waves, which is a function of distance and therefor results in a progressive overlapping between the opposing pressure boundaries as a function of distance.

A decay factor (b_{m_x}) derived specifically for an un-ducted sub-sonic rotor; based on spherical wave dispersion decay S_{m_x} (3.1) in conjunction with the expression for destructive interference $\mathrm{D_{m_x}}$ (Eq. 3.3) is given by b_{m_x} (3.4).

$$S_{m_x} = \sqrt{\frac{A_{0m}}{A_{x_m}}} \quad \text{: is the dispersion related decay factor} \qquad 3.2$$

$$\mathrm{D_{m_x}} = \cos\left(2\tan^{-1}\frac{0.25\lambda_{s_m}}{r_{x_m}}\right) \text{ :is the destructive interference factor} \qquad 3.3$$

$$b_{m_x} = \sqrt{\frac{A_{0m}}{A_{x_m}}}\left[1 - \mathrm{D_{m_x}}\right] \quad \text{Combined product decay function (pre tower interference)} \qquad 3.4$$

$$C_{m_x} = \sqrt{\frac{A_{0m}}{A_{x_m}}}\cos\left(2\tan^{-1}\frac{0.25\lambda_{s_m}}{r_{x_m}}\right) \quad \text{Combined for sum decay function (post interference)} \qquad 3.5$$

$$A_{x_m} = \pi r_{x_m}^2 \qquad 3.6$$

$$r_{x_m} = 0.25\lambda_{s_m} + 0.5x \qquad 3.7$$

Where:
A_{0_m} : is proportional to the area of the pressure wave at the rotor (i.e. (x) = 0) ref 3.2
A_{x_m} : is proportional to the pressure wave area at distance (x) from the rotor ref 3.2
x_T : is the axial distance between the rotor and the support tower
x_F : is the axial distance between the tower and the far field observation point.
$\tau = t - [\frac{c}{x_T + x_{F+}\, x_S}]$ is field real time relative to t which is rotor time (x_S is defined in section 5).
$\mathrm{p_B}$: is the blade surface differential pressure on blade B at radius (Z) divided by the highest value of (m) used in the Fourier series calculations (in the cases studied here this was 60).

The radius (r_{x_m}) of any given pressure wave (m) is a function of the distance (x) from the rotor plane (due to spherical dispersion) and is given by 3.7 (see Figure 3).

Distance (x) function destructive interference factor D_{m_x} (3.3) is calculated based on the ratio of the distance between the positive and negative pressure peaks at the source ($0.5\lambda_{s_m}$) for any given harmonic (m), and the dispersed diameter at distance (x) from the source of the pressure wave (m).
Since destructive interference will suppress the pressure pattern towards the inner radius of the rotating pattern more than the other areas of the overall pattern, the center of pressure (Z) will also expand as a function of distance such that:

$$Z_x = (Z + \frac{x}{2}) \qquad 3.8$$

(A_{x_m}):is related to the area of the dispersed pressure pattern of mode (m) at axial distance (x) from the rotor (Figure 3).

(A_{0_m}):is related to the area of the m[th] mode pressure pattern at the rotor (i.e. at (x) = 0).

When the axial decay factor from reference 1 (2.1) is applied to a hypothetical 3 blade ducted 1.6 MW wind turbine (40 meter radius blades and duct), the BPF decay rate is predicted to be about -34db at one radius axial distance (40 meters).
When equation. 3.4 is applied with identical parameters for an un-ducted rotor, the BPF decay rate is predicted to be about -17db at one radius axial distance.

3.3 Incorporation of the decay and interference factors into the expression for the pressure source 3.1

Equation 4.1 is an extension of the basic rotor pressure field equation (3.1), which incorporates the distance (x) related dispersion decay terms and the destructive interference terms.
A Fourier series ($\mathcal{F}R_{m_\tau}$), which represents the tower reflection interference has also been incorporated, this modulating factor will be discussed in detail in section 5.0.

$$p\ (\theta,\tau,x) = \sum_{m=1}^{\infty} [\, b_{m_{x_T}} \mathrm{p_i} \cos\big(m(\theta_i - \Omega\tau) + \phi_{m_i}\big)$$
$$+\mathcal{F}R_{m_\tau} b_{m_{x_T}} \mathrm{p_i} \cos\big(m(\theta_i - \Omega\tau) + \phi_{m_i}\big)]\, S_{m_{x_F}}$$
$$+[\mathcal{F}R_{m_\tau} C_{m_{x_F}} \mathrm{p_i} \cos\big(m(\theta_i - \Omega\tau) + \phi_{m_i}\big) - C_{m_{x_F}} \mathrm{p_i} \cos\big(m(\theta_i - \Omega\tau) + \phi_{m_i}\big)]$$

$$+\sum_{m=1}^{\infty} [\, b_{m_{x_T}} \mathrm{p_{ii}} \cos\big(m(\theta_{ii} - \Omega\tau) + \phi_{m_{ii}}\big)$$
$$+\mathcal{F}R_{m_\tau} b_{m_{x_T}} \mathrm{p_{ii}} \cos\big(m(\theta_{ii} - \Omega\tau) + \phi_{m_{ii}}\big)]S_{m_{x_F}}$$
$$+[\mathcal{F}R_{m_\tau} c_{m_{x_F}} \mathrm{p_{ii}} \cos\big(m(\theta_{ii} - \Omega\tau) + \phi_{m_{ii}}\big) - c_{m_{x_F}} \mathrm{p_{ii}} \cos\big(m(\theta_{ii} - \Omega\tau) + \phi_{m_{ii}}\big)]$$

$$+\sum_{m=1}^{\infty} [b_{m_{x_T}} \mathrm{p_{iii}} \cos\big(m(\theta_{iii} - \Omega\tau) + \phi_{m_{iii}}\big)$$
$$+\mathcal{F}R_{m_\tau} \mathrm{b_{m_{x_T}}}\ \mathrm{p_{iii}} \cos\big(m(\theta_{iii} - \Omega\tau) + \phi_{m_{iii}}\big)]S_{m_{x_F}}$$

$$+[\,\mathcal{F}R_{m_\tau}\,C_{m_{x_F}}\mathrm{p_{iii}}\cos(m(\theta_{iii}-\Omega\tau)+\phi_{m_{iii}})-C_{m_{x_F}}\,\mathrm{p_{iii}}\cos\big(m(\theta_{iii}-\Omega\tau)+\phi_{m_{iii}}\big)] \qquad 4.1$$

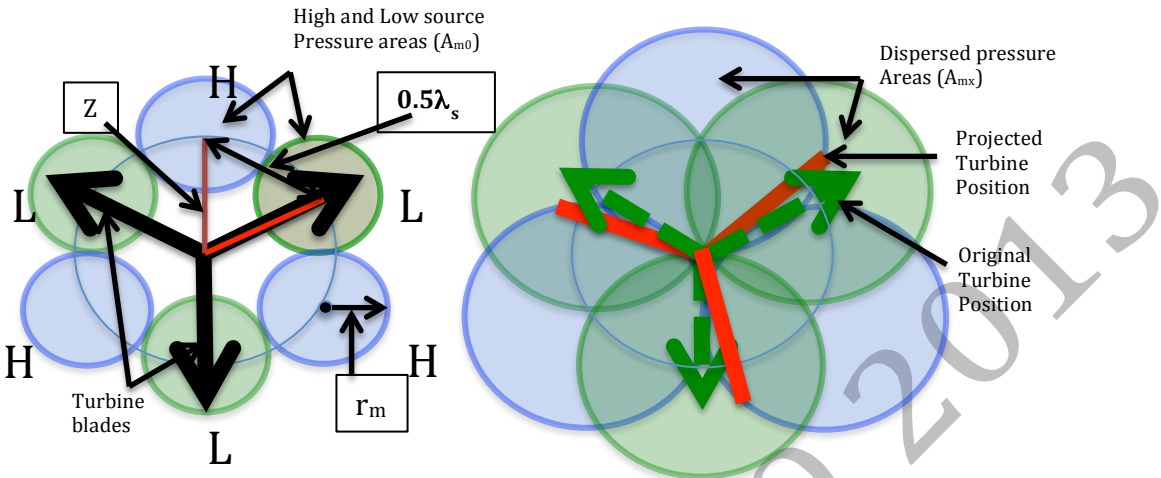

Figure 3

Figure 3 (left side) depicts a snap shot of the pressure pattern at the rotor plane for the fundamental only (m=3); The image on the right is similar and depicts a (spherical) plane rearward from the rotor plane approximately 100mS later (about 35 meters) and illustrates the progressive destructive interference between the highly coherent pressure waves from the rotor as they propagate away from the rotor. Also of note is the increase in the overall diameter of the rotor alone mode relative to the image on the left (rotor plane).

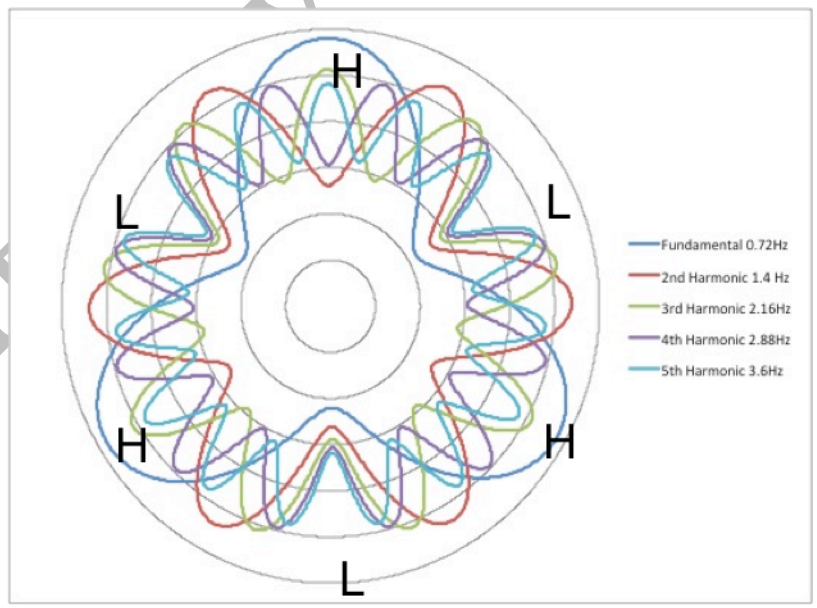

Figure 4

Figure 4 is a polar time function plot of the first 5 resultant Fourier components of equation 4.1 with an arbitrary (x) and no interaction effects, to show the representative High and Low pressure distribution around a circumferential path (Ref 1) This calculation was performed with m=1 to 60. Note that the m=1

Draft Dec 9 2013

and m=2 waves are cancelled out as are the harmonics of these waves (this will only happen completely when all 3 blade pressures (p) are equal).

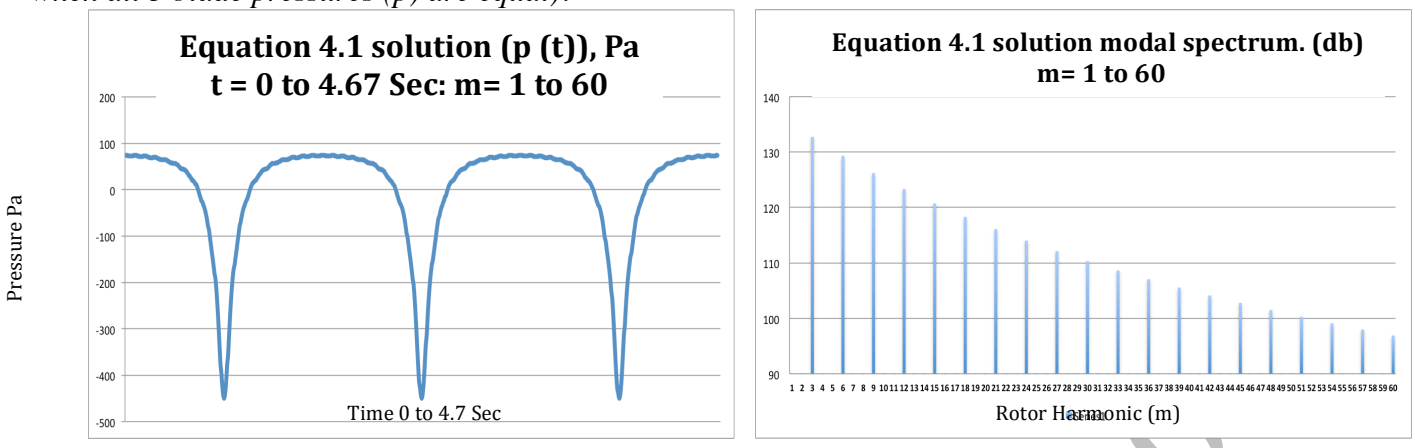

Figure 5

Figure 5 shows a time function graph (left) and frequency spectrum plot (right) showing the sum of the Fourier series of equation 4.1 for the 3-bladed rotor being modeled, at a distance of 8 m from the rotor plane (prior to tower interaction). These graphs represent the pressures that would be observed at a distance of 8 meters rearward from a hypothetical 1.6 MW wind turbine at a radius from the axis of 32 meters, at rated power based on the preceding hypothesis.

4-Rotor Stator Interaction

Probably the most significant discovery made in the Tyler Sofrin work was the effect of strut or reflector interaction with the rotor alone modes (Ref 1 Section 6.2 item 3.), which give rise to secondary spinning modes having the same frequencies as the rotor alone modes (including the blade passing frequency and all harmonics) but comprise numbers of pressure lobes ranging from 1 to theoretically an infinite number. The actual statement made in ref 1 pertaining to this reflection effect as one of the 3 sources of interaction noise was ”Interruption of the rotating periodic pressure field by the proximity of reflecting objects, apart from wake effects”.

The secondary modes spin at higher and lower angular rates than the rotor, depending on the number (n) of pressure lobes in the secondary pressure pattern, and is according to the relation $\omega_n = (m\Omega/n)$.

This relationship turns out to be important when n<m, because the spin velocity $(Z_n\omega_n)$ will be higher, resulting in some previously decaying modes becoming cut-on when $(Z_n\omega_n) \geq c$, This condition was demonstrated to result in propagation of those particular (cut-on) modes into the far field as opposed to the modes decaying close to the rotor as would be the case without the interaction condition.

It was shown in Reference 1, that for a single interference strut or reflector (as is the case for a wind turbine), $n = mB + k$: where k includes 0, all positive and negative integers $(-\infty < k < \infty)$: $k\ is\ an\ integer$ (Ref 1 Sect 6.0).

A negative resultant value for (n) indicates a negative spin direction relative to the rotor spin direction.

The frequencies observed for the secondary (interaction generated) spinning modes are identical to the rotor alone modes since $\omega_n n = m\Omega$, and $m\Omega = 2\pi f_m$.

Draft copy Dec 9 20

The interaction phenomenon was demonstrated experimentally during the Tyler Sofrin study and the governing principles are now, and have for some time been widely used in the gas turbine engine and fan industry to reduce radiated noise (ref 6.0).
It is evident that when the tangential velocity $(Z_n\omega_n)$ of any spinning mode pressure pattern C.P. (Center of Propagation: Ref 1) approaches (c), the circumferential wavelength (λ_s) approaches the free field wavelength (λ). At this condition, the propagation rate of the rotating pressure pattern in the circumferential direction is identical to the propagation rate in the axial direction (i.e. c). This condition physically prohibits the progressive superposition of the propagating (n) pressure waves, the related hypothetical destructive interference, and the attendant sound pressure level decay. The above set of physical conditions serves as a corollary to the hypothesis related to the decay of the rotor locked mode.

5.0 Rotor alone mode tower interaction

If an imaginary observer were fixed to one of the blades of the subject wind turbine, at about the 80% radius position, the tower as a reflecting object would be observed (by the observer) once per revolution of the rotor, as a brief reflecting pulse. A Fourier series can represent this reflecting pulse.
The magnitude of the reflection is a function of the area of the incident pressure wave (A_{x_m}) 3.6 in conjunction with the intersecting area (profile) of the reflecting tower (A_{T_m}), and the repetition duty-cycle; the reflection magnitude is given by:

$$Rl_m = D_T\, A_{T_m}/Z_m 2\pi A_{x_m} \qquad 4.2$$

Where (A_{T_m}): is the common or intersecting area between the tower surface and the pressure wave area (Figure 6), which is approximated by:

$$A_{T_m} = \sqrt[10]{\frac{1}{\left(\frac{1}{A_{x_m}}\right)^{10}+\left(\frac{1}{D_T 2r_{x_m}}\right)^{10}}} \qquad 4.3$$

: D_T is the tower diameter at the position corresponding to Z_{m_x}.

Since some portion of each of the pressure waves incident at the tower will be reflected (and scattered) in a forward direction, that portion of the wave will effectively be subtracted from the wave traveling past the tower into the far field, resulting in an interference interaction with the remaining propagating pressure pattern, including the destructive interference function responsible for nominally rapid decay of the rotor locked modes.
The complete Fourier series expression for the attenuation / interference effect as incorporated into (Eq. 4.1) is given by:

$$\mathcal{F}R_m\,(\psi,\tau) = \sum_{m=1}^{\infty} Rl_m \cos\big(m(\psi+\Omega\tau)\big) - Rl_m \qquad 4.4$$

Where:

Draft copy Dec 9 2013

$\psi = \theta_T - \theta_0 : (\theta_T)$ is the angular location of the tower relative to the observer angle (θ_0)

The tower reflection Fourier series $\mathcal{F}R_m$ (Eq. 5.3) is stationary relative to the rotor locked spinning pressure pattern and may be visualized in a similar way to the patterns shown in Figure 4 except the pattern is a stationary attenuating pattern, which interferes with the rotating pressure pattern. An interference pattern due to the Vernier effect (when the patterns have different m's), results from the difference between the stationary attenuation and rotating pressure patterns which is in fact what generates the so called Tyler Sofrin spinning modes (Ref 1 Sect 6.0).
Each of the large number of stationary patterns of $\mathcal{F}R_m$ interacts in this way with each of the rotor locked modes (Fig 4), resulting in a multitude of mostly decaying spinning modes, however, some of the spinning modes may rotate with sufficient velocity to attain the cut-on condition as has been previously described and has been demonstrated with other rotor systems (Ref. 1).
The spinning modes having n lobes (S_n) related to the hypothetical wind turbine are given by:

$$
\begin{aligned}
S_{n_{x_S}} = S_{n_x}\delta_{x_S} \sum_{n=-k}^{k} & \beta_{n m_{x_T}} \mathcal{F}R_{(m+n)_\tau} \mathrm{b}_{\mathrm{m_{x_T}}}\ \mathrm{p_i} \cos\left(m(\theta_i - \Omega\tau) + \phi_{m_i}\right) \\
& + \beta_{n m_{x_F}} \mathcal{F}R_{(m+n)_\tau}\ \mathrm{c}_{\mathrm{m_{x_F}}}\ \mathrm{p_i} \cos\left(m(\theta_i - \Omega\tau) + \phi_{m_i}\right) \\
& + \ \beta_{n m_{x_T}} R_{l_{m+n_\tau}}\ \mathrm{b}_{\mathrm{m_{x_T}}}\ \mathrm{p_{ii}} \cos\left(m(\theta_{ii} - \Omega\tau) + \phi_{m_{ii}}\right) \\
& + \beta_{n m_{x_F}} \mathcal{F}R_{(m+n)_\tau}\ \mathrm{c}_{\mathrm{m_{x_F}}}\ \mathrm{p_{ii}} \cos\left(m(\theta_{ii} - \Omega\tau) + \phi_{m_{ii}}\right) \\
& + \beta_{n m_{x_T}} R_{l_{m+n_{\psi\tau}}}\ \mathrm{b}_{\mathrm{m_{x_T}}}\ \mathrm{p_{iii}} \cos\left(m(\theta_{iii} - \Omega\tau) + \phi_{m_{iii}}\right) \\
& + \beta_{n m_{x_F}} \mathcal{F}R_{(m+n)_\tau}\ \mathrm{c}_{\mathrm{m_{x_F}}}\ \mathrm{p_{iii}} \cos\left(m(\theta_{iii} - \Omega\tau) + \phi_{m_{iii}}\right)
\end{aligned}
\qquad 4.5
$$

where:

δ_{x_S} : is an arbitrary decay factor (sect 6.0)
$\beta_{n m_x}$: is a velocity and radius related coupling factor (4.8, sect 6.0)
x_S : is the axial distance between the observation plane and (x_T)
n : is an integer where $(-\infty < n < \infty)$
S_{n_x} : is a decay factor related to the radial distance of the observer from $R_{\beta_{n_m}}$ (ref. 5.1)

$$R_{\beta_{nm}} = \frac{nC}{2\pi \mathrm{N} m} \qquad 4.6$$

The overall pressure field behind the hypothetical wind turbine is given by;

$p\ (\theta, \tau, x) + S_{n_{x_S}}$: (Eq. 4.1 & 4.5) figs 12 & 13 4.7

Draft copy Dec 9 2013

Figure 8 is a series of snapshots of polar time function graphs of the results of equation 4.5 for n=+1 and m= 6 illustrating the formation of a spinning mode as a result of the Vernier effect interference between the 7 lobe Fourier component generated by the reflection pulse effect of the tower, and a 6 lobed pressure pattern arriving from the rotor 8.5 meters away from the tower. To highlight the effect, time (τ) was fixed to the same period for each frame image while (ψ) was incremented (the tower location relative to the rotor was rotated) by 3.25 degrees per image (the 6 lobed pattern is not moving but the tower 7 lobed pattern is). The dashed line added to the time function graphs represents the average pressure of the pattern, and is what actually spins at the increased rate due to the Vernier effect interference. Note that the average pressure of the pattern actually rotates by 6 times (22.5 degrees per step) the incremented angle thus will spin at 6 times the rotational rate of the rotor locked pattern relative to the tower. It is this spinning of the average pressure of the pattern that is commonly referred to and measured as a spinning mode.

5.2 ~20Hz +harmonics Amplitude Modulated products.

It is highlighted that a portion of the pressure wave reflected forward from the tower will be incident to the passing blade surface, which results in a portion of the wave reflecting back toward the tower, resulting in a (somewhat inefficient) periodically excited resonant space (ref fig. 7). Scale measurements on a 1.6 MW turbine results in the distance between the blade and tower estimate at about 8.5 to 9.0 meters at the ~80% blade radius, which varies slightly as wind loading forces the blade towards the tower at higher wind speeds or power levels. The gap between the two reflecting surfaces form a half wave resonator when the blade is close to the tower, for frequencies of about 20Hz, 40Hz etc. and will result in some acoustic emission of these frequencies (ref fig 1) in conjunction with upper and lower sidebands at the BPF (the resonance is excited intermittently at the Blade Passing Frequency causing Amplitude Modulation and probably some Frequency Modulation of the resonance). The reflection coefficient (Rl_m) predicts a 46db reflection amplitude from the tower for m= 84 (20.1 Hz) and about 30db for m =168 (at rated power and wind speed), volumetric displacement effects of the moving blades will tend to increase the predicted pressure wave magnitude locally, however, these effects are not included in the model at this time. The resonance amplification factor has not been evaluated.
The amplitude-modulated resonance will also result in some lateral vibration (at the 20Hz + harmonics resonant frequencies) of both the tower and the turbine blade as the blade passes the tower.

Draft copy Dec 9 2013

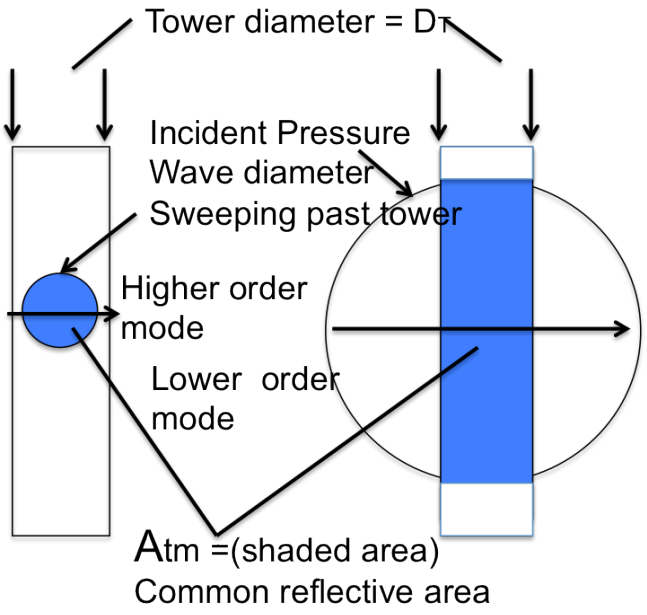

Figure 6 depicts the effective reflective area (A_{tm}) Used to calculate the reflection magnitude from given mode (ref. 5.1)

Figure 6

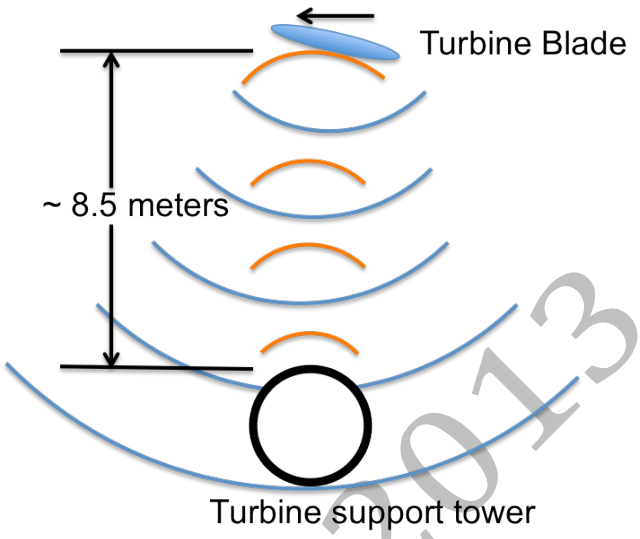

Figure 7 is a shcematic showing the resonant Space formed between the blade and tower As the blade passes the tower. The pressure Wave from the blade is reflected back toward The blade, resulting in further reflections.

Figure 7

Draft copy Dec 9 2013

6.0 Spinning Mode Radius Physical limitation

Evidently the maximum physical radius possible for any spinning acoustic mode is limited by the speed of sound (c) in the medium of propagation and is defined here as the propagation radius (R_β):

$$R_{\beta_{nm}} = \frac{nC}{2\pi \mathrm{N}m} : \text{(Eq. 4.6)}$$

Where: (n) is the number of spinning pressure lobes, (c) is the local speed of sound and Nm is the frequency in the stationary frame.

It is also evident from Reference 1 and the previous discussions of this study that there can be no sustained axial propagation of a spinning mode when the radius of its C.P. is less than the propagation radius (i.e. the mode is not cut-on and therefor decays). These two demonstrable features[*3] of spinning modes, imply a fixed and well-defined radius of propagation ($R_{\beta_{nm}}$) for any given propagating spinning mode (S_n). These two assertions imply that no distance related normal dispersion (Ref 5) of the pressure waves could be predicted.

Although no experimental measurements have been made in this study to confirm the propagation radius hypothesis, the computed radiation patterns of reference 1 (figure 20 of ref 1) and measurement data presented (Figures 21A and 21B of Ref. 1), support the hypothesis by showing the radius of the measurable SPL near the duct face, reducing as an inverse function of cutoff ratio ($\mathcal{E}$): where ($\mathcal{E}$) $= \frac{M^*}{M}$: $M^*$is the mode CP Mach number (The authors of reference 1.0 did not note this relationship).

6.2 Near field phase measurements

Phase measurement data recorded at close proximity to a wind turbine at ground level, which are presented in table 1.0, indicate phase angles between a pair of microphones (two sets of microphones were used) placed 50 meters apart, ~170 meters behind a wind turbine, approximately parallel to the rotor plane (shifts in the wind direction during the recordings will have resulted in errors in the parallelism of the microphone setup, which was not measured during the recordings).

The setup for the phase measurements is shown in Figure 9.

The measurements indicated modes of n=3 (fundamental BPF) n=4 and n=5 which were in all cases, non-propagating (decaying) interaction spinning modes at the interaction radius (the phase data for the BPF indicate that this mode is not in fact the rotor locked mode since phase polarity indicates counter rotation). These modes are the only modes detected at ground level, which may be an indication that these were the highest amplitude at the measurement location. This condition is predicted by the reflection coefficient having higher magnitudes at higher orders than lower orders, which results in higher spinning mode amplitudes for higher tower interference mode numbers (m+n), which results in the backward (counter rotating) spinning modes (n < 0) having higher amplitudes than the corresponding forward spinning modes (n > 0).

6.3 Coupling Coefficient

It follows that if there is no acoustic energy incident at the propagation radius (R_β) of a particular interaction (interference) generated mode, no propagating spinning mode could be established.

This condition may exist where a cut-off input spinning mode is incident at an interaction plane (i.e. the tower) with a C.P. radius minus a pressure wave radius ($Z_{m_x} - r_m$) > ($R_{\beta n}$), i.e. the inner most radius of the rotating pattern, being greater than the propagation radius ($R_{\beta n}$), or if ($Z_{m_x} + r_m$) <($R_{\beta n}$) for any number of resulting interaction modes (S_n) however more discussion / research on the effect of an increasing ($Z_{m_x} + r_m$) as a function of distance is required (ref section 7).

The condition ($Z_{m_x} - r_m$) > (R_{p_n}), may exist for upper harmonics from wind turbines depending on air temperature.

The second coupling limit ($Z_{m_x} + r_m$) < ($R_{\beta n}$) occurs for our hypothetical wind turbine when m < 5. At extremely cold conditions of about -60C the limit drops to m = 4. This limitation prevents the BPF (m=3) from ever becoming an interaction-spinning mode that will propagate. This fact may explain the noted absence of the fundamental BPF in measurements by at least 1 observer (ref 4 & fig 2).

As a result of the coupling coefficient the range of BPF harmonics that may normally result in propagating interaction spinning modes from our 3 blade hypothetical wind turbine is from 2 * BPF upwards although the amplitudes diminish significantly above about the 7th harmonic of BPF (m = 21 n =3) which will be lower than -20db below the 2nd harmonic spinning mode amplitude (ref fig 2 extreme far field measurements).

It cannot be stated that a coincidence between (Z_{x_m}) and (R_β) is a resonant condition, since no amplification is anticipated at the coincidence for an open rotor (Z_{x_m}) = (R_β), this is true contrary to considering the corresponding circumference ($2\pi R_{\beta_m}$) is an integral multiple of the free field wavelength (λ_m). However a resonant-like ~unity gain, coupling coefficient ($\beta_{n_{m_x}}$) has been formulated based on the energy availability at the propagation radius ($R_{\beta_{n_m}}$) and is incorporated into the expression ($S_{n_{x_S}}$) 4.4 representing the interaction spinning modes. ($\beta_{n_{m_x}}$) is a convenient method to filter out non-propagating interaction spinning modes from the results of (4.4), and is given by:

$$\beta_{n_{m_x}} = \frac{r_{m_x}}{\left(Z_{m_x} - R_{\beta_{n_m}}\right)^2 + r_{m_x}} \qquad 4.8$$

Where: $R_{\beta_{n_m}} = \frac{nC}{2\pi \mathrm{N} m}$ (ref 4.6)

Draft copy Dec 9 2013

6.4 Interaction Spinning Modes radiated from the hypothetical wind turbine

The spinning modes themselves are a result of the interference between the relatively stationary Fourier pattern set up between the tower, and the rotating rotor alone Fourier series (Fig 8).

Decay rate of spinning modes.

The decay rate of sub-sonic spinning modes (the rotor alone modes for example) is governed by a combination of dispersion (spherical spreading) and destructive interference, both of which are active features in the decay of the rotor alone modes.

The decay rate of free field sonic spinning modes appears to be in question, since the propagation radius cannot increase without violating the sonic velocity limit (and presumably conservation of energy prevents the waves from simply vanishing).

This constraint appears to discount spherical spreading and its related SPL decay as it is presently defined (the SPL measurements made at 125 Km distance also support this hypothesis, see Fig 2 and Ref 4). The destructive interferences between wave fronts in a given pattern in the direction of propagation are also eliminated since the spinning modes in any given mode from a single turbine are mutually coherent (sourced by the same rotor system).

It is not reasonable to expect that there will be zero decay in SPL of a spinning mode and it seems logical that the energy in the spinning mode will at the least, dissipate as a function of time, and will presumably be influenced by atmospheric conditions.

Pending further research in this area, and for the purpose of this study, an arbitrary decay function (δ_{x_S}), which is an exponential function of time, has been assigned. No consideration is given to atmospheric effects although this will obviously need consideration before the amplitude of propagating spinning modes at any given distance will be accurately predictable.

It is assumed that radiation pattern of infrasound from the spinning mode in a radial direction will be similar to an Archimedean Spiral (Fig. 10); which is expected to decay as a function of distance (S_{n_x}) from the mode radial location as a line source (-3db per doubling of radial distance).

$$\delta_{x_S} = e^{-\left(\frac{x_S}{kc}\right)} \qquad \text{is an axial exponential decay factor} \qquad 4.9$$

Where: k is a time constant, which based on extreme far field data has been arbitrarily set at 120 seconds.

$$\left(S_{n_x}\right) = \frac{.5\lambda_n}{x_S + .5\lambda_n} \qquad \text{where } (x_S) \text{ is the radial distance from the mode radius } (R_{\beta_{n_m}}) \qquad 5.1$$

Draft copy Dec 9 2013

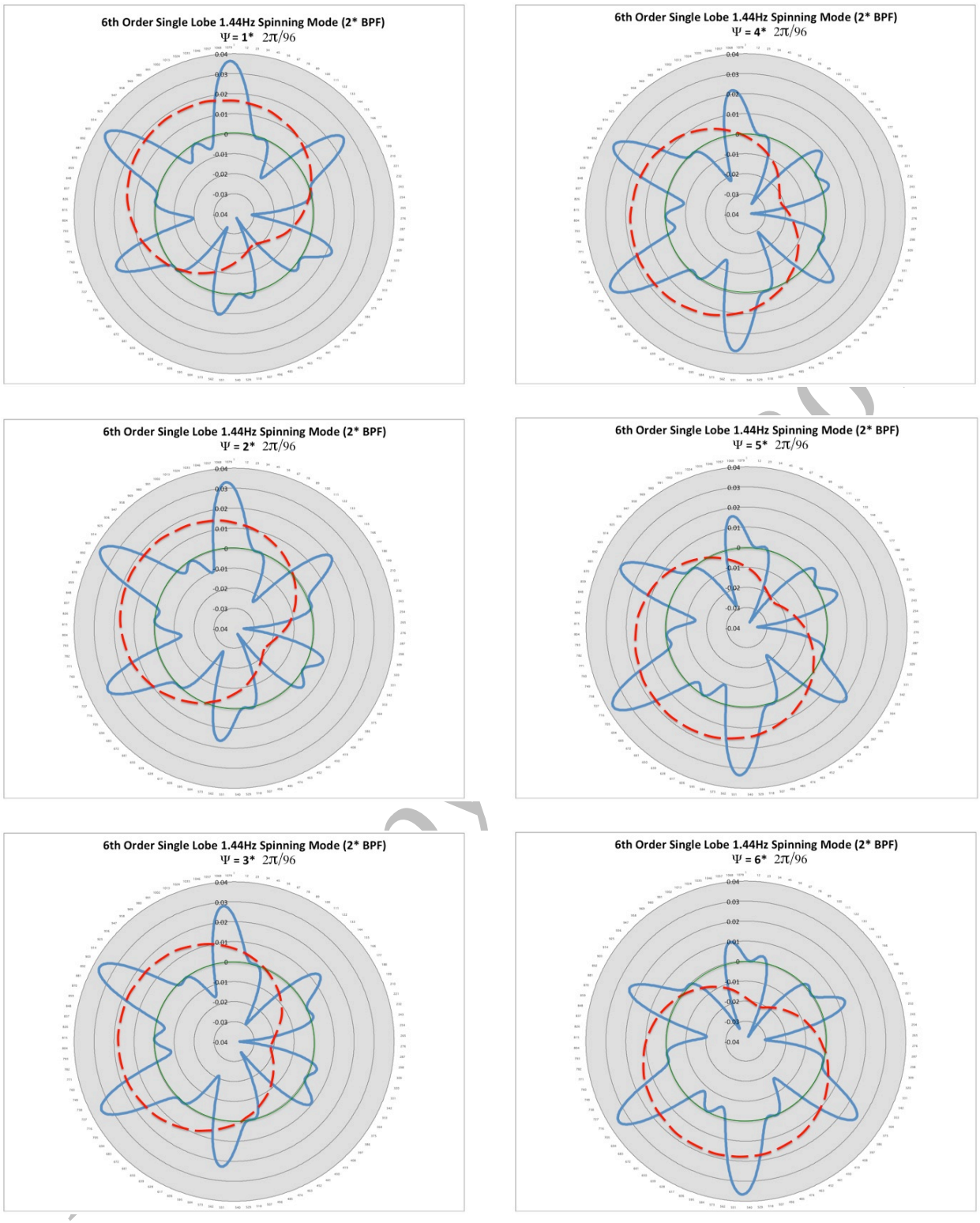

Figure 8

The images of figure 8 are the results from equation 4.2 for m+n=7 and m=6 resulting in a single lobed mode, rotating in the opposite direction of the rotor (in this case in the same direction as the tower relative to the rotor).

For each of the images, starting at the top left down, then top right down, ψ is incremented By 3.75 degrees (CCW) while the time period for each frame is held constant, to show the rotation of the average pressure profile as a result of the interference of the 6-lobe pressure pattern with the 7 lobed tower Interference pattern, this result is what is referred to as a spinning mode.

Distance between microphone groups is 50 Meters

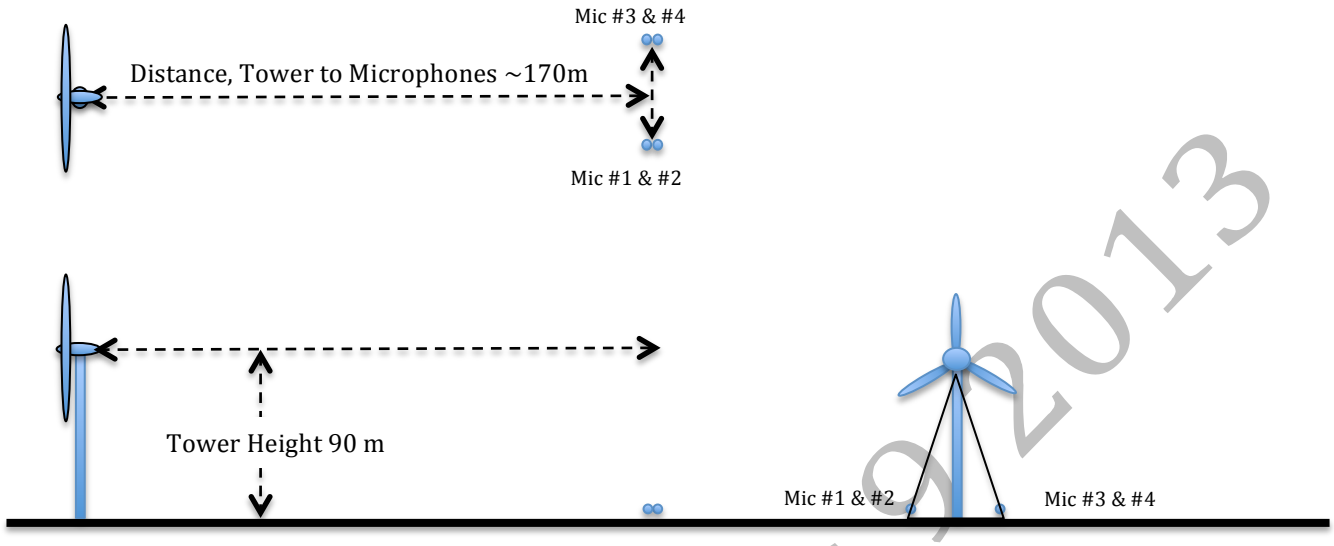

Figure 9

Frequency	Rotor Mode (m)	ϕ Mic # 2 Degrees	ϕ Mic # 3 Degrees	ϕ Mic # 4	Average ϕ 3 & 4	Calculated lobe number (n) = ϕ / A	Ideal ϕ (for (n))	Error %	Notes
0.72 Hz	3	1.269	92.70	96.17	94.43	3.0 (3)	93.12	+1.38	BPF
1.44 Hz	6	-2.648	134.22	136.5	135.36	4.36 (4)	124.16	+9.07	2nd H
2.16 Hz	9	-2.480	129.34	129.82	129.58	4.17 (4)	124.16	+4.18	3rd H
2.88 Hz	12	-0.825	118.42	121.38	119.9	3.86 (4)	124.16	-3.55	4th H
3.6 0Hz	15	-2.403	162.00	164.44	163.22	5.25 (5)	155.2	+4.91	5th H
4.32 Hz	18	-4.289	121.11	120.34	120.72	3.89 (4)	124.16	-2.85	6th H

Table 1.0
Phase Measurement Results and Calculated Spinning Mode lobe numbers (n)

The angle (A) is the physical angle formed between the axis of the turbine and the two microphone sets (ref fig 9). $(A) = 2\arctan\left(\frac{25\ meters}{90\ meters}\right) = 31.05\ Deg.$

The average phase angle (ϕ) is between the reference microphone (1) and microphone 3&4 averaged. The existence of a phase angle in this measurement beyond that which could be explained by plane wave propagation between the two microphone sets (also no plane wave is expected perpendicular to the rotor plane) is evidence that spinning modes are present. That the lobe number (n) is only equal to the mode number (m) in the case of the fundamental proves that other than the BPF mode, these are interaction-generated spinning modes. Based on conventional phase notation, the BPF mode (0.72 Hz row in Table 1) and all other mode phase polarities indicate that all detected modes are counter rotating modes (phase of 3 and 4 are leading 1 and 2 whereas the rotor rotation is counterclockwise looking from the rear of the turbine where the microphones are located).

Draft copy Dec 9 2013

None of the modes detected would be calculated as being cut-on at the interaction zone radius of ~27 - 32 meters. That the magnitude of phase angles is measurable at the radius of measurement may be explained by either the assumption that decaying interaction spinning modes transition into an Archimedean spiral radiation pattern, or that decayed interaction modes cut-on at ($R_{\beta_{n_m}}$) and then radiate in an in Archimedean spiral radiation pattern from that radius. Further research and measurements are required in this area to gain a more complete understanding.

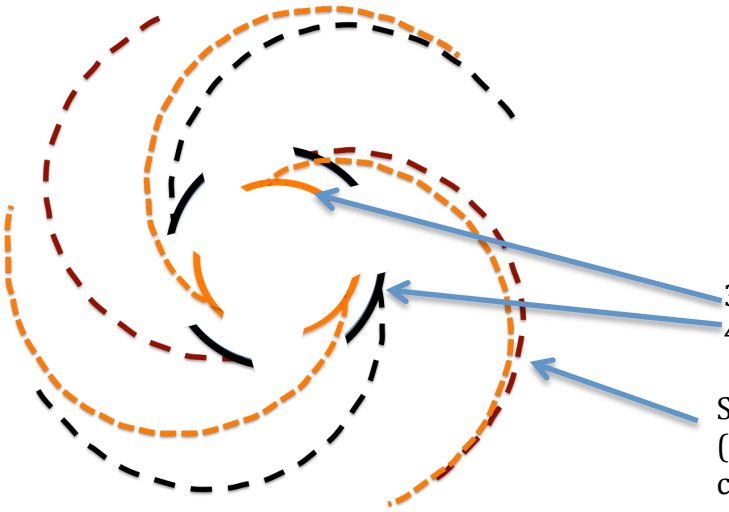

Figure 10

Archimedes Spiral radiation pattern viewed looking in the axial direction toward the turbine.

Figure 10 shows three and four arm Archimedes spiral patterns depicting the radial acoustic radiation from two fixed radii ($R_{\beta_{n_m}} = \frac{nC}{2\pi Nm}$) spinning modes.
In this example and the notional diagram representing it, both modes have the same frequency but differ in lobe numbers thus spin rate (angular frequency), the three lobe mode will spin about 33.3% faster than the 4 lobe mode, (Ref. Section 4).

Phase measurements using two pairs of microphones ~170 meters behind a wind turbine are tabulated in Table 1 with the test layout shown in Figure 9.

Draft copy Dec 9 2013

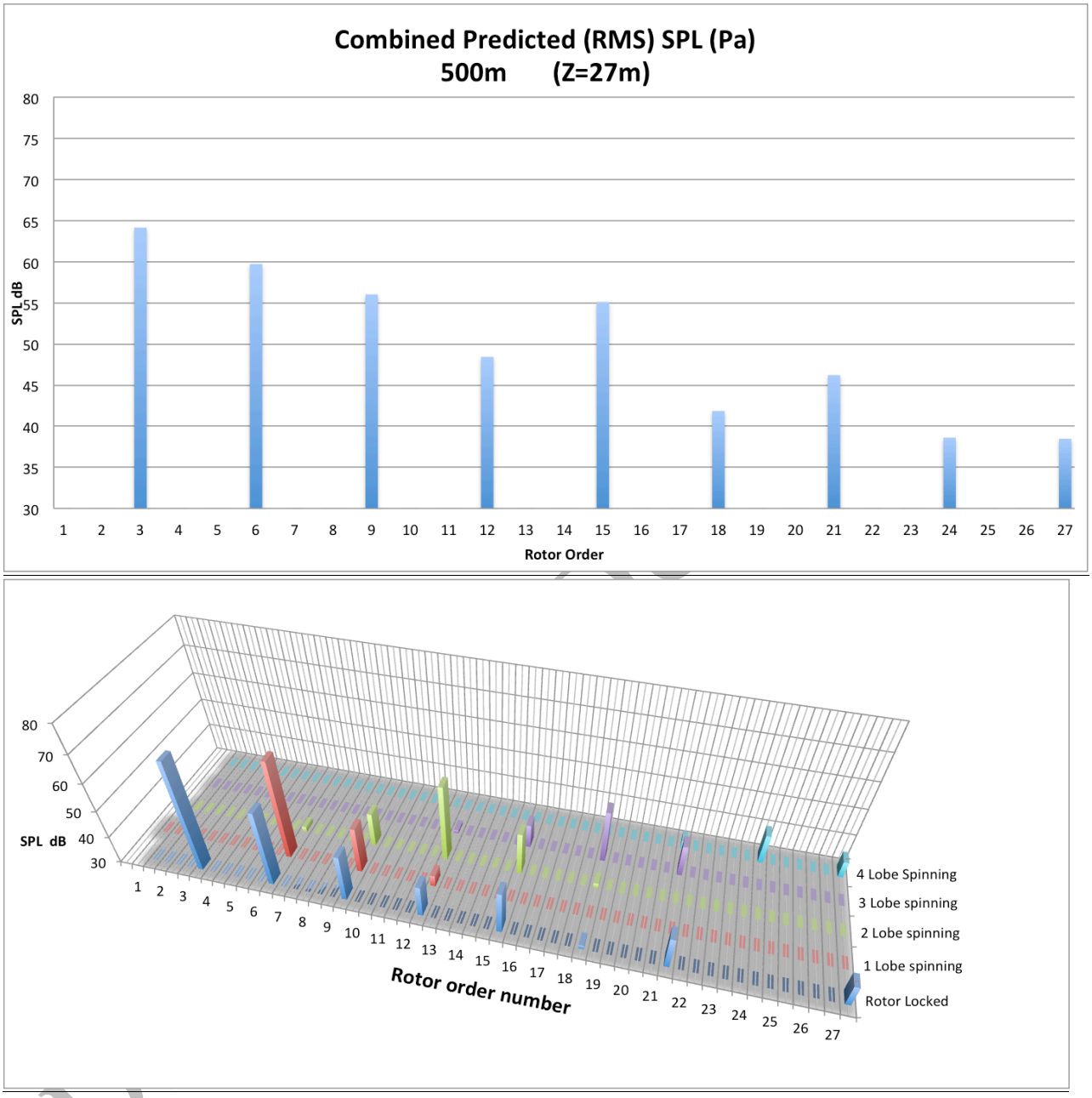

Figure 11

The 3D spectrum plot directly above shows the predicted rotor locked mode in the front row of the graph (Eq. 4.1 converted to dB. the x axis is rotor harmonic number m), each subsequent row behind the first shows the magnitudes of the predicted propagating spinning modes as calculated by equation 4.5 and converted into db. For example the highest calculated amplitude spinning mode, is the 1 lobe mode from the sixth rotor mode (second harmonic of BPF): Note that there is no propagating spinning mode predicted for the BPF frequency. The spectrum plot above the 3D spectrum plot shows the combined amplitudes as would be measured by a microphone (RMS value of all modes at each frequency). Both the upper and lower graphs of figure 11 were calculated at an axial displacement of

500 meters (tower located 8.5 meters from the rotor plane) and observation radial offset of 90 meters (ground level), with an assumed power output of 1.6MW and Z (center of pressure) of 32 meters radius. The data's trend agreement of Figure 11 was improved significantly (Fig. 12) by adjusting the center of pressure radius (Z) downward to 27 meters from the originally assumed radius of 32 meters. This improvement was primarily due to improved coupling of the 9th (3* BPF) order mode into $R_{\beta_{nm}}$.

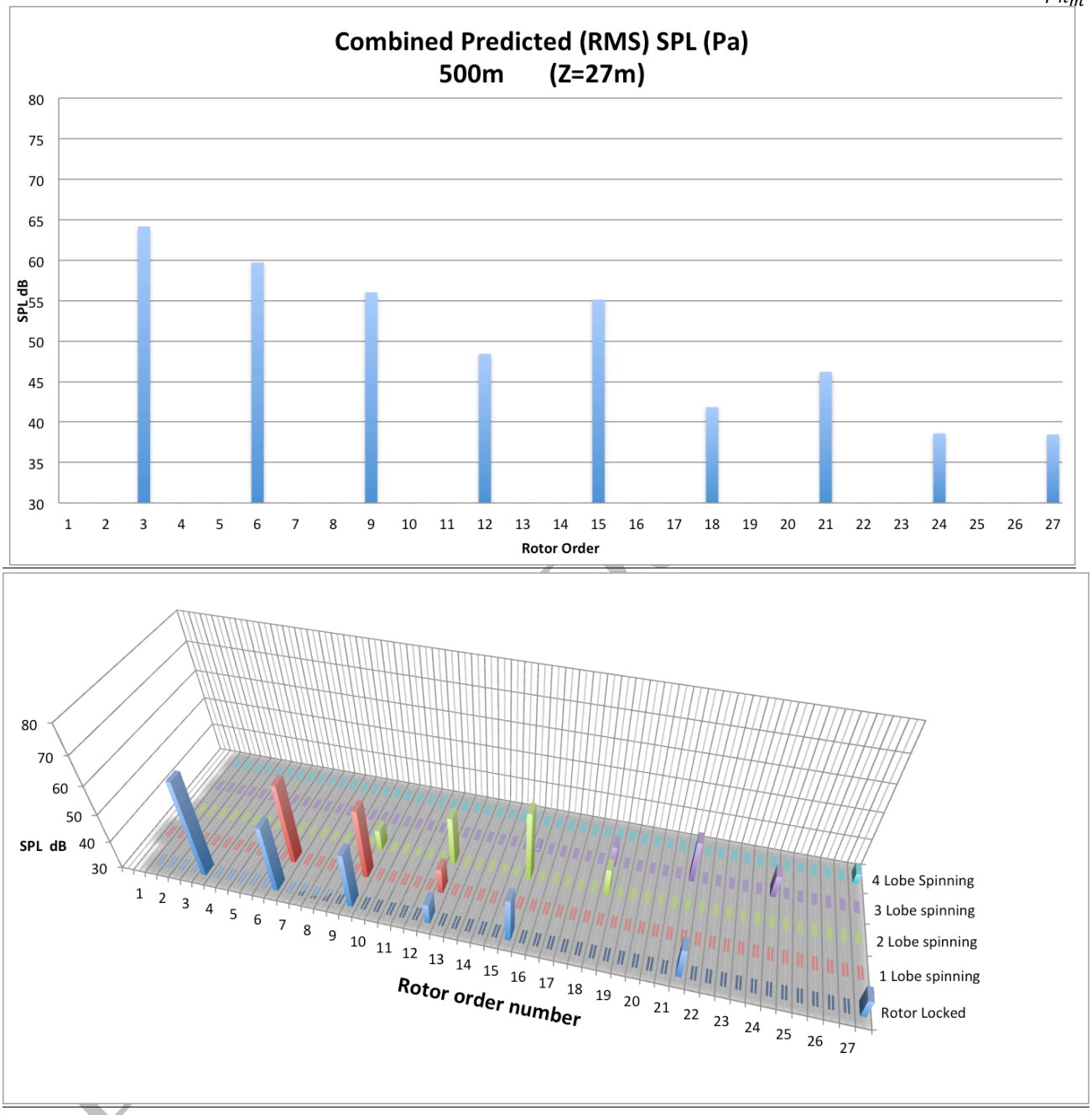

Figure 12

Figure 12 shows the results using the same parameters as were used for Figure 11 results with the exception that the center of pressure parameter has been reduced to 27 meters as opposed to the originally assumed value of 32 meters. Far better agreement with the measured trends (Figure 1) was achieved with 27 meters as the pressure center on the rotor, since the 9th (3* BPF) spinning mode coupling to $R_{\beta_{nm}}$ was improved, and the magnitude of the rotor locked modes were reduced slightly as well.

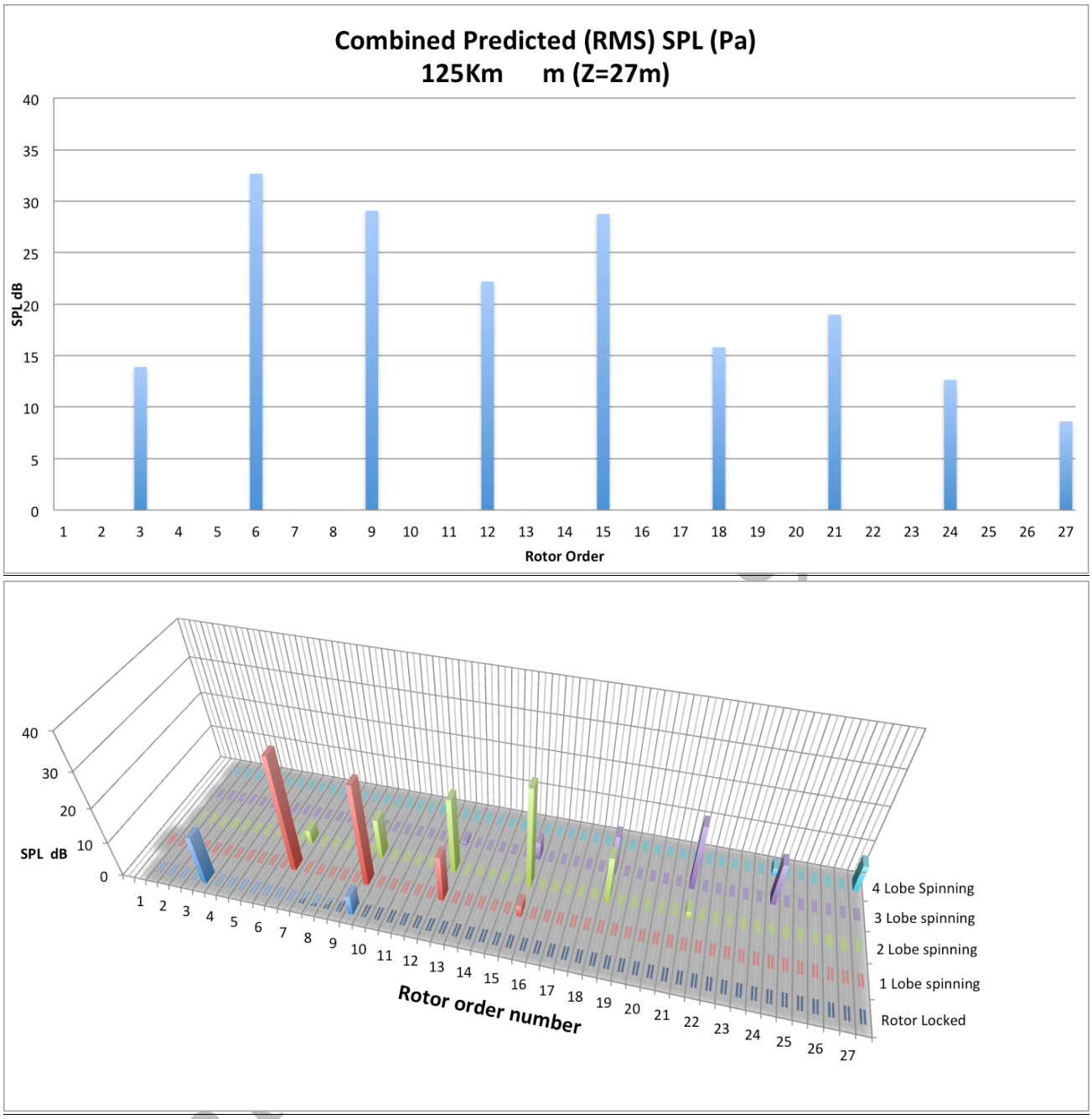

Figure 13

Figure 13 is based on the same parameters as Figure 12 results, except that the axial observation distance (x_F and x_S) has been increased to 125 Kilometers. The amplitude decay of the rotor locked modes is very significant with the BPF reduced by about 50db and harmonics of the BPF rotor locked modes decaying by more than that. The spinning modes are predominant because no spherical spreading or destructive interference decay is predicted in this model, with only an arbitrary time function exponential decay included. The data in the combined amplitude plot of Figure 13 compares favorably with data recorded ~125 Kilometers from the closest wind turbine in Parry Sound, Ontario (Fig. 2 & Ref. 4). Of particular interest is the agreement on the very low magnitude of the 3rd order mode (BPF) which can not attain a cut-on condition through interaction (a single lobed mode at the BPF will only spin 3 times the rotor speed, the base rotor speed center of pressure velocity, is less than Mach 0.15 and as such would need to increase by a factor of at least 6 for any portion of the mode to achieve a cut-on condition.

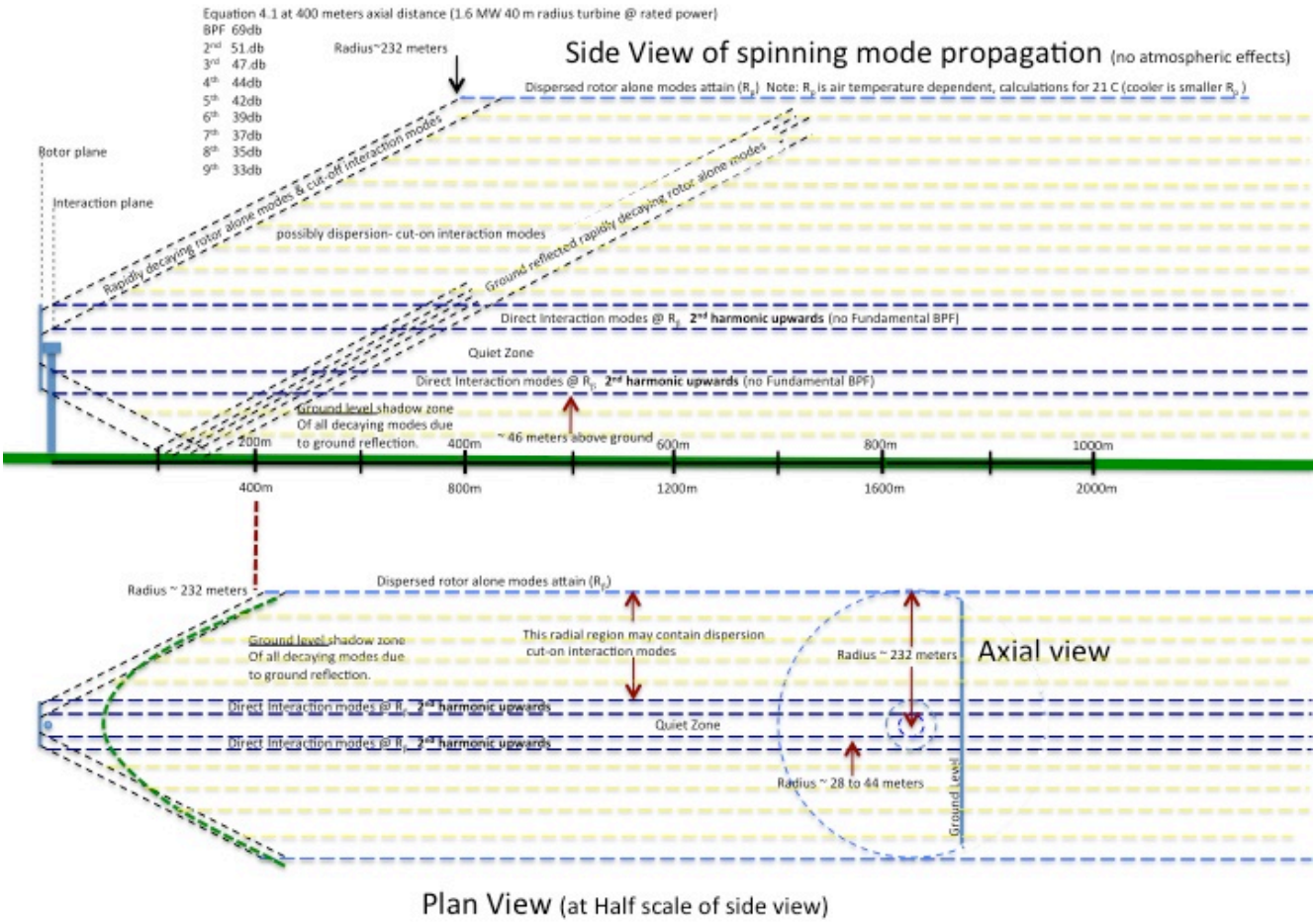

Figure 14

Figure 14 upper image provides an overall side view of the propagation patterns that the formulations and hypothesis of this study imply, A shadow zone from approximately 160 meters behind the turbine is the result of ground reflection of the decaying rotor locked modes, however, decaying interaction spinning modes and Archimedean pattern radiation from the cut on spinning modes will be measurable at greater axial distances from the turbine in the shadow zone and into the extreme far field.
The lower image of Figure 14 is a plan view but at half the scale, with an axial view for reference.
The amplitudes marked in this diagram were based on Z=32 m and will be ~ 6db lower for Z=27 m.

Draft copy

7.0 Summary

The fundamental processes through which the generation of spinning modes, from a hypothetical wind turbine is generated have been examined and formalized, through the application of Fourier series.

A hypothesis, which proposes an explanation for the rapid decay of rotor locked modes while simultaneously explaining the generation of propagating spinning modes by acoustic interference, has been presented.

The source of low frequency noise (~20 Hz AM harmonic series) is predicted as a side effect of the spinning mode generation process, the mechanism described may suggest potential amplitude

reduction techniques for the resulting 20 Hz harmonic series noise (which however may not reduce the spinning mode magnitudes).

Data which has been generated using the equations developed (Figures 12 and 13), compares well to close range measurements (~ 500 meters) shown in this study, in measurements made by others (Fig 1, Ref: 2.0 and Ref 4.0), and also to measurements made at over 125 Km from the closest wind turbine (Fig. 2 and Ref. 4 data).

A concept related to the propagation radius of acoustic spinning modes based on well-known gas laws (velocity of sound c) has been presented. The concept indicates that the SPL decay rate of propagating spinning modes is less than what would be predicted from a point source based on either spherical or cylindrical spreading at a similar frequency's.

This conclusion is supported by measurement data from extreme far field microphones where at over 125 km distance to the closest wind turbine, BPF harmonics are measured at SPL's of ~30db (Figure 2, Ref. 4 data) while at distances of ~ 1km the levels are typically less than ~55db (Figure 1 and Ref. 2 and Ref. 4), however, extreme far field levels may not yet be accurately predictable. Further research is required to better understand the SPL decay characteristics of low frequency free field spinning modes with respect to dissipation and atmospheric influences.

The phase measurement data presented in Table 1 indicates that interaction spinning modes are generated, and that none of the spinning modes measured at ground level would be cut-on modes at the interaction zone. However, the phase measurement data raises the question as to the nature of the decaying spinning modes transition through ($R_{\beta_{n_m}}$) as a result of spherical spreading. The radius of the phase measurement location (~90m) is > $R_{\beta_{n_m}}$ for the 4th 5th and 6th harmonic of BPF.

That the phase angles were detected between the microphones at the measurement radius, indicates that the decaying spinning modes have either transitioned to a cut–on condition at ($R_{\beta_{n_m}}$) and radiate radially forming an Archimedean spiral pattern from the propagation radius ($R_{\beta_{n_m}}$) <u>or</u> the decaying spinning modes have transitioned from a decaying spinning mode into an Archimedean spiral radiation pattern.

Evidence that the decaying spinning modes achieve a cut-on condition as they attain the propagation radius ($R_{\beta_{n_m}}$) as a result of spherical spreading (i.e. due only to the increase in Z_{m_x}) has not been documented, however the phenomenon has not been ruled out. Further field measurements and research is required to understand better the effect on a "near to cut-on" mode as its radius increases with distance (time) and the free field spinning mode phenomenon in general, since this will potentially influence far field infrasound levels of higher power wind turbines.

*[3] *The concept related to an upper radius limit (R_p) was not discussed in reference 1.0, however the concept of a limited radius presented here is in full agreement with ref 1.0 formulations, this can be shown if one considers a case where the duct radius is just less than ($R_{\beta_{n_m}}$) limiting the radius of the mode to less than($R_{\beta_{n_m}}$) where axial propagation of the spinning mode rapidly decay's. Increasing the radius of the duct beyond ($R_{\beta_{n_m}}$) for precisely the same rotor conditions, will allow the same mode to propagate in the axial direction essentially un-attenuated. This can be confirmed through the formulations of ref 1.0 where the circumferential wavelength was derived as* $\lambda_s = \frac{2\pi r_0}{m}$*: where* ($r_0$) *is duct wall radius and (m) is the number of pressure lobes in the circumferential pressure pattern.*

Draft copy Dec 9 2013

REFERENCES

[1] J. M. Tyler and T. G. Sofrin "Axial Flow Compressor Noise Studies," SAE Technical Paper 620532, 1962, doi:10.4271/620532.

[2] B. Walker, G.F. Hessler Jr., D. M. Hessler, R. Rand, P. Schomer. "A cooperative measurement survey and analysis of low frequency and infrasound at the Shirley wind farm in Brown County,Wisconsin. Report Number 122412-1.

[3] W. Richarz and H. Richarz "Wind turbine noise diagnostics" technical paper presented at Inter-noise, August 23-26 2009 Ottawa, Canada.

[4] A. Metelka "Narrow Band low frequency pressure and vibration inside homes in proximity to wind farms" ASA Conference, San Francisco Dec 3 2013.

[5] J.R. Hassall and K. Zaveri "Acoustic Noise Measurements" Bruel & Kjaer, June 1988.

[6] J. D. Kester and G. F. Pickett "application of Theoretical Acoustics to the Reduction of Jet Engine Noise" 1972 Journal of applied physics Volume 5 number 1

Draft copy Dec 9 2013